

Magnetohydrodynamic (MHD) effects on conjugate mixed convection in a triangular enclosure with swirling reactive fluid: A computational approach

Arman Habib Polash, Hamim Faisal, Daud Hasan, Md. Abdur Rahim Hera, Ahmed Imtiaz Rais,
Md. Jisan Mahmud*

Department of Mechanical Engineering, Hajee Mohammad Danesh Science and Technology University, Dinajpur 5200, Bangladesh

ARTICLE INFO

Keywords:

Conjugate heat transfer
Mixed convection
Magnetohydrodynamics
Internal heat generation/absorption
Rotating cylinder

ABSTRACT

In this research, we investigate the quantitative characteristics of conjugate mixed convection heat transfer, internal heat generation/absorption due to chemical reaction and the magnetohydrodynamic impact on a lid-driven right-angled triangular enclosure which has a solid circular cylinder situated at the center. The perpendicular edges of the enclosure remain stationary and maintain a constant cold temperature. The tilted side is adiabatic, while the bottom edge slides uniformly, maintaining a constant elevated temperature. The solid cylinder was rotated at different angular velocities in clockwise and counterclockwise directions while applying a constant magnetic field to the enclosure. By varying the Reynolds ($31.623 \leq Re \leq 316.23$), Richardson ($0.1 \leq Ri \leq 10$), Grashof number ($10^3 \leq Gr \leq 10^5$), internal heat generation or absorption coefficient ($-10 \leq \Delta \leq 10$), and the rotating cylinder's speed ($-2 \leq Re_c \leq 2$) along with a given magnetohydrodynamic effect of the cylinder, parametric simulation is used. Plots of streamlines and isotherms are used to depict qualitative results. In contrast, the average Nusselt number, normalized Nusselt number, and average drag coefficient are used to calculate the configuration's quantitative thermal performance and flow characteristics. To the best of our knowledge, this study is the first to present a comprehensive numerical investigation of conjugate heat transfer in a lid-driven triangular enclosure that simultaneously considers: (1) magnetohydrodynamic effects, (2) both clockwise and counterclockwise rotation of an internal solid cylinder, and (3) internal heat generation and absorption. The results reveal a strong interactive influence among these factors. Most notably, internal heat absorption enhances the average Nusselt number by up to 74.5 % and reduces the average drag coefficient by 89 % when both Reynolds and Grashof numbers are at their maximum values. Parallel to this, streamline and isotherm plots show overall heat distribution and flow separation within the enclosure. The simulations clearly show that higher Reynolds and Grashof numbers, combined with internal heat absorption, markedly enhance heat transfer, while the effect of cylinder rotation remains relatively minor.

1. Introduction

Mixed convection is a sophisticated thermo-fluid phenomenon that is induced by the coincidence of forced and natural convection in a specific domain at the same time. This consists of complex interactions between mechanically induced fluid movement and buoyancy effects influenced by thermal gradients. It has been very important in many technical applications; some include food processing technologies, heat exchangers, nuclear reactor systems, solidification processes, and solar energy collectors (Ali et al., 2022). The most recent investigations (Selimefendigil and Öztop, 2017) have explored how internal heat is

produced and absorbed by processes of electric current flow in liquids, heat generated and absorbed through chemical reactions (endothermic and exothermic) at interfaces of a given system, operations in nuclear reactors, and other physical phenomena associated with heat generation/absorption. For example, the passage of an electric current through a saline solution generates heat internally. Therefore, it is necessary to include the internal heat generation and absorption while predicting the thermal transport performance of the thermo-fluid systems.

Solar collectors, electrical equipment, and building roof design are just a few examples of engineering applications that rely on mixed convection heat transfer in triangular enclosures (Chamkha et al., 2018). Temperature gradients within fluid-filled enclosures often lead to the

* Corresponding author.

E-mail addresses: arman.habib.polash19@gmail.com (A.H. Polash), hamimf13@gmail.com (H. Faisal), daud.hasan597@gmail.com (D. Hasan), hera.me@hstu.ac.bd (Md.A. Rahim Hera), intiaz.me@hstu.ac.bd (A.I. Rais), jisanmahmud.me@hstu.ac.bd (Md.J. Mahmud).

Nomenclature	
A	Dimensionless area of the fluid domain
A_m	Amplitude
B_0	Magnetic Field Strength
C_d	Average Drag Coefficient
C_p	Specific Heat Capacity (J/kg-K)
d	Diameter of Cylinder (m)
g	Gravitational Acceleration (m/s ²)
Gr	Grashof Number
Ha	Hartmann Number
k	Thermal Conductivity (W/m-K)
L	Length of the Side of the enclosure (m)
Nu	Average Nusselt Number
p	Pressure (Pa)
P	Non-Dimensional Pressure
Pr	Prandtl Number
Q	Internal Heat Generation (W/m ³)
Re	Reynolds Number
Ri	Richardson Number
T	Temperature (K)
u, v	Velocity Components (m/s)
U, V	Dimensionless Velocity Components
u_o	Top Lid's Sliding Velocity (m/s)
u_p	Cylinder's circumferential velocity (m/s)
x, y	Cartesian Coordinates (m)
X, Y	Dimensionless Cartesian Coordinates
N	Nondimensional Wall-Normal Distance
Greek Symbols	
ϵ	Error (%)
β	Thermal Expansion Coefficient (1/K)
λ	Oscillation number
Δ	Thermal Heat Generation Coefficient
Θ	Dimensionless Temperature
μ	Dynamic Viscosity of fluid (Pa.s)
ρ	Density of fluid (kg/m ³)
Ω	Cylinder Speed Ratio
ω	Cylinder's Rotational Speed (Rad/s)
Subscripts	
av	Average
c	Cold
h	Hot
nor	Normalized
f	Fluid
s	Solid
Abbreviation	
CCW	Counter Clockwise
CW	Clockwise
MHD	Magnetohydrodynamics

development of convective flow. Thus, many studies have focused on mixed convection in common enclosure shapes, such as rectangular, square, or triangular enclosures. The enclosure's movable lid improves heat transmission and fluid circulation rates. Numerous studies (Selimefendigil and Öztop, 2017; Chamkha et al., 2018; Shahid et al., 2021) have investigated mixed convection in lid-driven triangular cavities under a variety of heating conditions. In general, research on this topic can be divided into two categories. Differentially heated enclosures with horizontal wall (top/bottom) moving at a constant speed fall under the first category. The second category comprises studies that focus on triangular enclosures, featuring a side wall moving at constant velocity and internal temperatures that vary spatially. Selimefendigil and Öztop (Selimefendigil and Öztop, 2017) investigated mixed convection in a partially heated triangular cavity filled with nanofluid, finding that as forced convection became dominant, overall heat transfer declined—an effect they alleviated by incorporating nanoparticles. Similarly, Chamkha et al. (Chamkha et al., 2018) studied magnetohydrodynamic mixed convection in a triangular cavity with a moving wall and observed a decline in heat transfer under forced-convection-dominated conditions. Shahid et al. (Shahid et al., 2021) examined the combined results of natural and forced convection within an isosceles triangular enclosure under various controlled conditions. They found that the spontaneous convective flow was transferring heat at a faster pace.

Several studies have delved deeper into the magnetohydrodynamic (MHD) effects on convective heat transfer in lid-driven enclosures (Uddin et al., 2015; Selimefendigil et al., 2016; Çolak et al., 2020; Oztop et al., 2011; Al-Salem et al., 2012). Uddin et al. (Uddin et al., 2015) and Selimefendigil et al. (Selimefendigil et al., 2016) examined lid-driven enclosures under an applied magnetic field. Their findings indicated a magnetic field's effect can impede convective flow, thereby reducing rates of heat transmission. There are a large number of effects that magnetic fields have on various technological purposes and energy storage applications, like the purification of molten metal, microelectromechanical systems, cooling systems in nuclear reactors, and crystal growth processes. The transport of convective heat can be

regulated by an external magnetic field. Lorentz force produces more secondary vortices in a cavity, and a strengthening of the magnetic field results in a commensurate decrease in heat transmission, according to Eren Çolak et al. (Çolak et al., 2020), who conducted an excellent examination of the magnetohydrodynamic effect. A higher magnetic field results in more uniform isotherms and a higher mean cavity temperature. After comprehensive analyses of the mixed convective flow's thermal and flow characteristics under the influence of magnetohydrodynamics, the velocity field and the heat fields were found to be significantly impacted by the applied magnetic field's intensity, as noted by Hakan F. Oztop et al. (Oztop et al., 2011) and Al-Salem et al. (Al-Salem et al., 2012).

According to the findings of the above-stated research works, the majority of lid-driven enclosures did not have internal obstructions. Subsequent studies (Khanafer and Aithal, 2013; Haq et al., 2020; Soomro et al., 2020; Xiong et al., 2021; Younis et al., 2023; Hussain et al., 2023) also suggested that with the addition of a cylindrical body to the various forms of enclosures like square, hexagonal, triangular, etc., the heat transfer rate increases tremendously. Heat transfer rates were shown to rise in differentially heated square and hexagonal enclosures when fixed circular obstructions were present, as reported by Khanafer & Aithal (Khanafer and Aithal, 2013) and Haq et al. (Haq et al., 2020), respectively. Soomro et al. (Soomro et al., 2020) observed comparable outcomes. They also found that introducing a circular object into a lid-driven, partially heated triangular enclosure enhanced heat as well as thermal efficiency. In another investigation, Hussain et al. (Hussain et al., 2023) examined the effects of installing four heaters in the four quadrants of the cylindrical cavity and found an increase in fluid velocity along a particular corner.

Nevertheless, in the case of comparing the mixed convection of a stationary cylinder, it was found that there was an improvement in the flow circulation and overall heat transfer related to a revolving circular cylinder within an enclosed area that was differently heated (Costa and Raimundo, 2010; Liao and Lin, 2014; Mamun et al., 2023; Selimefendigil et al., 2019; Aissa et al., 2024; Amine et al., 2021). Selimefendigil et al. (Selimefendigil et al., 2019) have conducted one of the

finest studies in their work. The impact of varying cylinder rotational speeds and directions was the focus of the study. It demonstrated how a cylinder rotated counterclockwise enhanced heat transfer and enabled simultaneous fluid rotation. One such research study is reported by Aissa et al. (Aissa et al., 2024), which found that increasing the speed of the cold cylinder at the enclosure causes the same increase in thermal activity at the hot wall that leads to increased heat transfer and vorticity. Likewise, the study on existing literature by Amine et al. (Amine et al., 2021) revealed that an increase in the dimension of the cylinder within the enclosure led to increased heat transfer performance.

Recent investigations (Islam et al., 2024; Mahmud et al., 2022; Paul et al., 2021; Rasel et al., 2023; Chowdhury et al., 2021; Hasan and Saha, 2024; Chatterjee et al., 2014; Javed and Saha, 2023; Tasnim et al., 2023; Rahman et al., 2010) have revealed that conjugate heat transfer, involving heat transfer in both solids and fluids, is influenced significantly by the enclosure's geometry and boundary requirements, particularly when an obstacle or heat-conducting object is introduced. As an illustrative example, a numerical investigation was also carried out by Mahmud et al. (Mahmud et al., 2022) to assess the effect of volumetric heat generation on mixed conjugate convection in a square cavity that is differently heated. The study also showed that the rotational orientation of the solid cylinder and its angular velocity had a minimal impact on the total system's thermal characteristics. Furthermore, Rasel et al. (Rasel et al., 2023) explored how different parameters affect rotational speed and significantly increase heat transfer efficiency when studying convective flow within a vented square cavity with spinning cylinders. Table 1 summarizes key facts about conjugate mixed convection in the early literature on solid cylinders. In this instance, the following symbols are used to represent the corresponding dimensionless parameters: Grashof number (Gr), cylinder speed ratio (Ω), Prandtl number (Pr), Richardson number (Ri), Reynolds number (Re), side cavity length (L), and cylinder diameter (d).

Internally heat-generating or absorbing convective heat transfer has attracted great interest recently because of its various applications in geophysical and energy engineering fields. Some examples are the conduction of electric currents by semiconducting fluids such as glass and electrolytes, heat recovery from large-scale geothermal storage systems, radiative cooling of molten glass, nuclear fuel debris cooling, and heating flowing water in solar collectors (Chamkha, 2002). Chamkha (Chamkha, 2002) concluded that volumetric heat generation led to a decrease in heat transmission in the case of promoting flow inside a side lid-driven enclosure that was differentially heated. Nonetheless, Sivasankaran et al. (Sivasankaran et al., 2014) observed that introducing a corner heater within the top lid-driven square cavity significantly enhanced thermal performance when volumetric heat generation was present. Numerous researchers (Hasan et al., 2024; Saha, 2015; Mahmudi et al., 2014; Selimefendigil and Öztop, 2016; Abu Bakar et al., 2020; Imtiaz Rais et al., 2023; Hasan and Saha, 2024) consistently discovered that regardless of the cavity's design, heat generation and absorption have a major influence on the heat transfer process. An interesting research study done by Imtiaz Rais et al. (Imtiaz Rais et al., 2023) investigated the process of heat generation and absorption in a top-lid-driven cavity with a rotating solid object within it. They found that improved heat transmission rate and even temperature distribution within the enclosure are both significantly impacted by heat absorption.

Besides, Hasan et al. (Hasan and Saha, 2024) found that the combined influence of an intensified magnetic field (MHD), elevated lid velocity, and buoyancy forces greatly enhances the heat transfer rate. They also mention that internal heat generation behaves as a thermal-resisting factor, the flow of heat through it being lower while significantly influencing fluid temperature profiles, entropy generations, and thermal efficiency.

To date, no previous study has examined the combined magnetohydrodynamic (MHD) effects on conjugate mixed convection in a bottom lid-driven right-angled triangular enclosure filled with a swirling reactive fluid. In particular, the simultaneous influence of an external magnetic field, volumetric heat generation/absorption (ion conducting/chemical reaction), and an internally rotating cylinder has not been addressed. The present computational study fills this gap by systematically varying the cylinder's rotational speed and direction, the internal heat generation/absorption coefficient, and the applied magnetic field strength over representative Grashof, Richardson, and Reynolds number regimes. Streamline and isotherm plots provide qualitative insight into the flow and thermal fields, while average and normalized Nusselt numbers and drag coefficients quantify the enclosure's thermal performance. These results will guide the design of engineering systems—such as rotating machinery, heat exchangers, chemical reactors, and solar collectors—where swirling reactive fluids under mixed convection and MHD conditions demand efficient thermal management.

2. Physical model

Fig. 1 illustrates the right-angled, triangular-shaped geometry of side

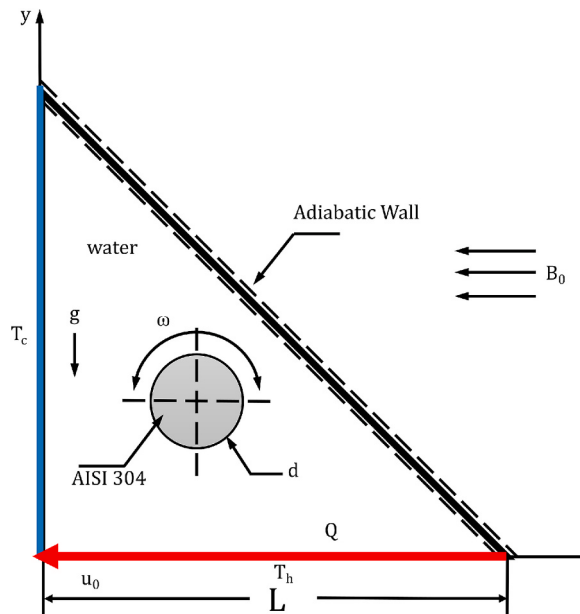


Fig. 1. Diagram of a right-angled, triangular-shaped geometry of side lid-driven cavity with a revolving solid cylinder that is propelled by a lid.

Table 1

An overview of research that has been published on conjugate mixed convection in different solid cylinder enclosures:

Authors	Sliding lid	Quantity of cylinder	Working fluid	Ri	Gr	Re	d/L	Ω
Islam et al. (Islam et al., 2024)	None	1	Air	0.1–10	10^3 – 10^5	32–316	0.2–0.4	None
Mahmud et al. (Mahmud et al., 2022)	Top	1	Water	0.1–10	10^3 – 10^5	31.623–316.23	0.2	-0.1,0.1
Paul et al. (Paul et al., 2021)	Left	2	Air	1	10 – 2.5×10^6	10–500	0.1–0.4	0.025,50
Rasel et al. (Rasel et al., 2023)	None	2	Air	31.623–316.23	0.1–10	10^4	0.2–0.4	-3,3
Chowdhury et al. (Chowdhury et al., 2021)	Left, Right	2	Air	1	$10^{2.4}$ – 10^6	10–2000	0.2	-5,5
Hasan et al. (Hasan and Saha, 2024)	None	1	Water	0.1–10	10^3 – 10^5	31.623–316.23	0.25	-1,1
Chatterjee et al. (Chatterjee et al., 2014)	Left	1	Air	0.1–10	10^3 – 10^5	100	0.2	-5,5

length L enclosed in a Cartesian coordinate system with known boundary conditions. The bottom lid of this enclosure is kept at a higher temperature T_h (where $T_h > T_c$) and moves uniformly in a negative x-direction with a velocity of u_0 . The vertical wall temperature is maintained at T_c , while for the inclined wall it is at an adiabatic condition. A solid cylinder fabricated from stainless steel (AISI 304) is situated inside the center of the enclosure. The diameter of the cylinder is represented by d , while its thermal conductivity, k_s , is 14.9 W/mK. It rotates at ω , either clockwise or counterclockwise. The definition of the cylinder's peripheral velocity is $u_p = \omega d/2$. The enclosure water's working fluid has a thermal conductivity of $k_f = 0.61$ W/mK and a Prandtl number of $Pr = 5.85$. Gravity acts in a vertical downward direction. Apart from this, the system incorporates the rate of internal heat generation or absorption in the working fluid, which is represented as Q (W/m³). Finally, there is an application of magnetic field intensity, B_0 , uniformly applied to the negative x-direction across the entire system.

3. Mathematical model

The continuity of mass, momentum conservation, and energy conservation serve as the study's governing equations. The continuous, two-dimensional laminar flow in an enclosure containing Newtonian, incompressible fluids with constant thermophysical parameters is the subject of the current investigation. The analysis neglects radiation effects and viscous dissipation while assuming density variations induced by temperature differences (Boussinesq approximation). Under such conditions, the following mathematical formulation is set for the problem (Mahmud et al., 2022):

Fluid domain:

$$\frac{\partial x}{\partial y} + \frac{\partial u}{\partial y} = 0 \quad (1)$$

$$\rho(u \frac{\partial u}{\partial x} + v \frac{\partial u}{\partial y}) - \mu \left(\frac{\partial^2 u}{\partial x^2} + \frac{\partial^2 u}{\partial y^2} \right) + \frac{\partial p}{\partial x} = 0 \quad (2)$$

$$\rho(u \frac{\partial u}{\partial x} + v \frac{\partial u}{\partial y}) - \mu \left(\frac{\partial^2 u}{\partial x^2} + \frac{\partial^2 u}{\partial y^2} \right) + \frac{\partial p}{\partial y} - \rho g \beta (T - T_c) + \sigma B_0^2 v = 0 \quad (3)$$

$$\rho C_p (u \frac{\partial T}{\partial x} + v \frac{\partial T}{\partial y}) - k_f \left(\frac{\partial^2 T}{\partial x^2} + \frac{\partial^2 T}{\partial y^2} \right) - Q = 0 \quad (4)$$

Solid domain:

$$k_s \left(\frac{\partial^2 T}{\partial x^2} + \frac{\partial^2 T}{\partial y^2} \right) = 0 \quad (5)$$

In the Cartesian coordinate system, x and y represent the spatial coordinates. In contrast, velocity coordinates are provided by u and v . Other variables are T for temperature, p for pressure, B_0 for magnetic induction, and g for gravitational force. Water, as a heat transfer fluid, possesses dynamic viscosity (μ), density (ρ), the coefficient of thermal expansion (β), and the specific heat capacity at constant pressure (C_p). In the subsequent analysis, the respective variables are scaled appropriately using suitable factors (Equation (6)) to normalize the problem described in Equations (1)–(5).

$$[U, V] = \frac{[u, v]}{u_0}, [X, Y] = \frac{[x, y]}{L}, P = \frac{p}{\rho u_0^2}, \Theta = \frac{T - T_c}{T_h - T_c}, \Delta = \frac{QL^2}{K_f(T_h - T_c)} \quad (6)$$

Where U and V symbolize the non-dimensional velocity components in the X and Y directions respectively, moreover, the non-dimensional pressure and temperature are symbolized by P and Θ , respectively, whereas Δ signifies the internal volumetric heat absorption/generation coefficient. The following dimensionless equations are generated when the governing equations are modified to include the aforementioned dimensionless scales:

Fluid domain:

$$\frac{\partial U}{\partial X} + \frac{\partial V}{\partial Y} = 0 \quad (7)$$

$$U \frac{\partial U}{\partial X} + V \frac{\partial U}{\partial Y} - Pr \left(\frac{\partial^2 U}{\partial X^2} + \frac{\partial^2 U}{\partial Y^2} \right) + \frac{\partial P}{\partial X} = 0 \quad (8)$$

$$U \frac{\partial V}{\partial X} + V \frac{\partial U}{\partial Y} - Pr \left(\frac{\partial^2 V}{\partial X^2} + \frac{\partial^2 U}{\partial Y^2} \right) + \frac{\partial P}{\partial Y} - Ri\Theta + Ha^2 Pr V = 0 \quad (9)$$

$$U \frac{\partial \Theta}{\partial X} + V \frac{\partial \Theta}{\partial Y} - \left(\frac{\partial^2 \Theta}{\partial X^2} + \frac{\partial^2 \Theta}{\partial Y^2} \right) - \Delta = 0 \quad (10)$$

Solid domain:

$$\frac{k_s}{k_f} \left(\frac{\partial^2 \Theta}{\partial X^2} + \frac{\partial^2 \Theta}{\partial Y^2} \right) = 0 \quad (11)$$

Thereby, k_f denotes the thermal conduction of the fluid phase, while accordingly, k_s is denoted as the thermal conduction of the solid cylinder. In terms of dimensionless parameters, it includes the Hartmann number (Ha), Grashof number (Gr), Reynolds number (Re), Prandtl number (Pr), and Richardson number (Ri) underneath equations (8)–(10). These parameters whose definitions have been defined in equation (12) are useful in characterizing the thermal and fluid dynamic aspects of the system.

$$Ha^2 = \frac{\sigma B_0^2 L^2}{\mu}, \quad Gr = \frac{\rho^2 g \beta (T_h - T_c) L^3}{\mu^2}, \quad Re = \frac{\rho u_0 L}{\mu}, \\ Pr = \frac{\mu C_p}{k_f}, \quad Ri = \frac{Gr}{Re^2} \quad (12)$$

The interface and dimensionless boundary conditions used in this research are summarized in Table 2. Here, X_c and Y_c will specify the non-dimensional coordinates of the cylinder center, Re_c stands for the rotational Reynolds number, and N for the dimensionless distance orthogonal to the wall. The value of Re_c is computed based on the peripheral velocity (Mahmud et al., 2022) of the cylinder and the diameter, as specified in equation (13).

$$Re_c = \frac{\rho u_p d}{\mu} = \frac{\rho \omega d^2}{2\mu} \quad (13)$$

The following describes the system's border and interface criteria (14)–(17):

Inclined wall:

$$U = 0, V = 0, \frac{\partial \Theta}{\partial N} = 0 \text{ at } Y = -X + 1 \text{ and } 0 \leq X \leq 1 \quad (14)$$

Perpendicular wall:

$$U = 0, V = 0, \Theta = 0 \text{ at } X = 0 \text{ and } 0 \leq Y \leq 1 \quad (15)$$

Bottom wall:

$$U = 1, V = 0, \Theta = 1 \text{ at } Y = 0 \text{ and } 0 \leq X \leq 1 \quad (16)$$

For cylinder:

Table 2
Criteria for the system's boundaries and interface that were used in the study:

Parameters	Cylinder Surface	Horizontal wall	Inclined wall	Vertical wall
Θ	$(k_s/k_f)(\partial \Theta / \partial N)_s =$ $(\partial \Theta / \partial N)_f$	1	$\partial \Theta / \partial N =$ 0	0
U	$2(Y - Y_c)(Re_c/Re)/(d/L)$	1	0	0
V	$2(X - X_c)(Re_c/Re)/(d/L)$	0	0	0

$$U = 2(Y - Y_c)(Re_c/Re)/(d/L), V = 2(X - X_c)(Re_c/Re)/(d/L), \Theta = K(\partial\Theta/\partial N)_s = (\partial\Theta/\partial N)_f \text{ at } (X - X_c)^2 + (Y - Y_c)^2 = (d/2L)^2 \quad (17)$$

The average drag coefficient (C_d) for the sliding lid, the normalized Nusselt number (Nu_{nor}), and the average Nusselt number (Nu) of the hot edge can all be defined as follows (Mahmud et al., 2022):

$$Nu = \int \frac{\partial\Theta}{\partial Y} \Big|_{Y=0} dX, \quad Nu_{nor} = \frac{Nu(Re_c \neq 0)}{Nu(Re_c = 0)}, \quad (18)$$

$$C_d = \frac{2}{Re} \int_0^1 \frac{\partial U}{\partial Y} \Big|_{Y=1} dX$$

It uses the subscripts “s” and “f” respectively, to indicate the solid and fluid domains.

4. Numerical procedure

4.1. Discretization method

This work uses a segregated finite element solution approach based on the Galerkin weighted residual formulation to solve the dimensionless governing equations (7) – (11) under the boundary conditions listed in Table 2. The finite element method enforces Dirichlet boundary conditions by directly assigning U, V, and Θ values to nodes on the enclosure walls. For the rotating cylinder, a no-slip condition is imposed by defining its tangential velocity components in the global Cartesian framework, proportional to the angular velocity (ω) and referenced to the cylinder's center coordinates. By discretizing the computational domain into triangular elements as shown in Fig. 2, this method successfully approximates solutions to partial differential equations of complex geometry. The governing nonlinear equations of mass, momentum, and energy are converted into algebraic systems through the Galerkin weighted residual method. These equations are linearized using Newton's method and solved sequentially via direct triangular factorization. To achieve numerical accuracy, convergence is monitored by tracking the residual norms for each governing equation and the relative change in all field variables. Iterations continue until all residuals fall below a prescribed tolerance (e.g., 10^{-3}) and the relative

changes in successive iterates remain below this threshold. This discretization strategy thus promises rapid convergence and yields reliable precision results.

4.2. Mesh strategy and grid independence study

To establish confident and precise numeric outcomes, the whole computational triangulated model consisted of solid and fluid sub-domains using a triangular structured non-uniform mesh with different dimensions. Special attention was given to mesh refinement in critical regions such as the rotating cylinder surface and the enclosure walls. In these areas, a significantly denser mesh was employed by introducing inflation layers and smaller triangular elements. This approach ensured the accurate resolution of steep velocity and temperature gradients, particularly near boundaries, allowing precise capture of boundary layer development and shear-driven flow characteristics. A grid independence analysis was conducted on the average Nusselt number to determine how the results are affected by changes in the level of mesh density. The findings showed that additional refining had little effect on the average Nusselt number after a certain number of elements. The generated meshes were therefore deemed sufficient to accurately capture the intricate details of heat distribution and fluid dynamics within the enclosure. Table 3 summarizes the findings of the grid refinement study, utilizing the evaluation criteria of the average Nusselt number. Various mesh configurations, from extremely coarse to extremely fine, were tested to determine the optimal mesh resolution. Ultimately, an “extra fine” mesh consisting of 15,115 elements was chosen as it shows negligible deviations in the average Nusselt number. Hence, it is confirmed to be sufficiently capable of providing accurate results. Further specifications about the selected “extra fine” mesh are in Table 4. The outcomes of this investigation are graphically depicted in Fig. 3, wherein the incremental element number is utilized to illustrate the variation of the Nusselt number along with the corresponding error (ϵ). The computational error in this analysis is determined in the following way (Tasnim et al., 2023):

$$\epsilon = \left| \frac{Nu_c - Nu_i}{Nu_c} \right| \times 100\% \quad (19)$$

The Nu_i and Nu_c are the individual and converged Nusselt numbers, in the context of numerical simulations.

4.3. Model Authentication

Before initiating the parametric solution of the proposed numerical simulation model, the results from the model were compared with the results published by Mahmud et al. (Mahmud et al., 2022) and Rahman et al. (Rahman et al., 2010). In particular, the reference model used to compare the outcomes of the current model was the conjugate mixed convective water flow investigation by Mahmud et al. (Mahmud et al., 2022) in a square enclosure with internal heat generation. Fig. 4 provides the quantitative confirmation of the model for two different rotational directions, showing a fairly good correlation between the

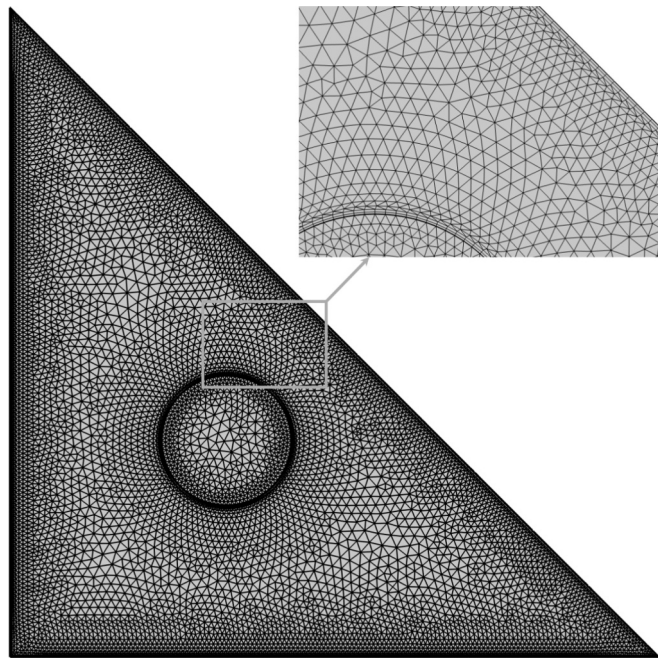


Fig. 2. The mesh distribution strategy employed in the study was developed through a grid refining procedure.

Table 3

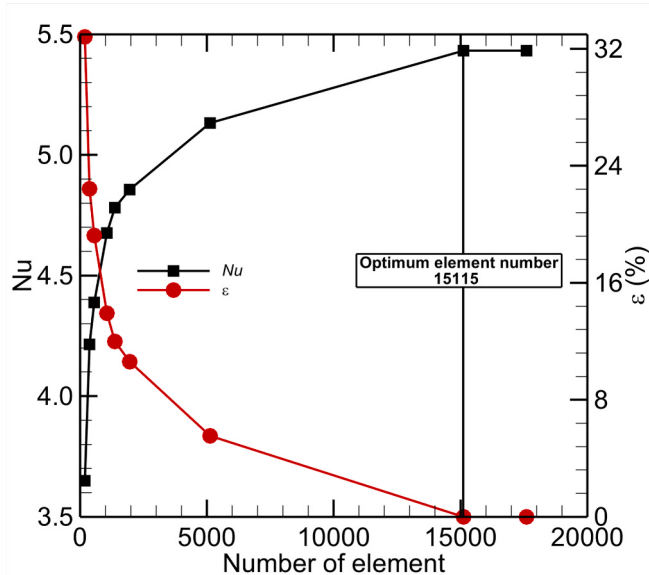
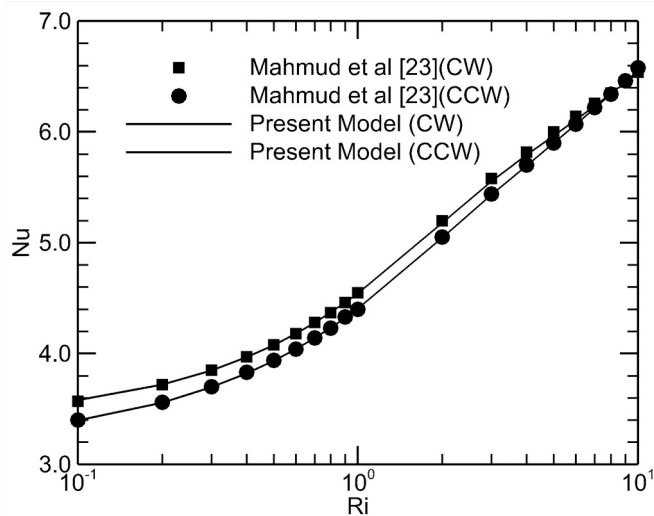
Grid refinement analysis based on Nu for $Gr = 10^5$, $Re_c = 2$, $Re = 100$, $\Delta = 10$, $k_s/k_f = 24.43$, $d/L = 0.2$, $Pr = 5.85$, and $Ha = 10$:

Mesh	Node Number	Element Number	Nu
Extremely Coarse	142	193	3.649
Extra Coarse	256	371	4.214
Coarser	368	557	4.388
Coarse	666	1056	4.676
Normal	855	1371	4.781
Fine	1187	1955	4.856
Finer	3004	5129	5.131
Extra Fine	8417	15,115	5.432
Extremely Fine	9658	17,597	5.431

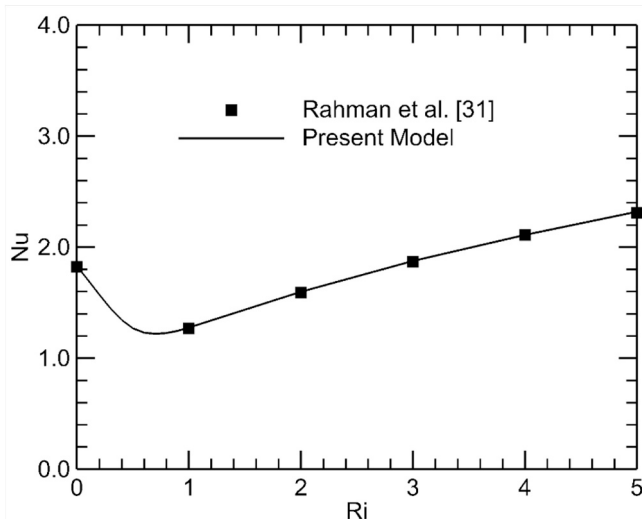
Table 4

Thorough details regarding the ideal mesh type selected (Extra fine).

Details on the Mesh	Statistics of Meshes
Quantity of elements	
Triangles	13,909
Quads	1206
Number of nodes	8417
Edge Elements	607
Vertex Elements	7
Overall	15,115
Average elements quality	0.7987

**Fig. 3.** The grid refinement study and the identification of the appropriate number of elements for this investigation.**Fig. 4.** Results from Mahmud et al. (Mahmud et al., 2022) and the current model are compared, demonstrating how \bar{Nu} varies with Ri for $Re = 100$, $Pr = 5.85$, $k_s/k_f = 24.43$, $\Delta = 10$, $d/L = 0.2$, $Re_c = \pm 2$.

numerical predictions and the available data.

For validation, the error (e) between the present model and reference studies is calculated using the formula from (Tasnim et al., 2023):**Fig. 5.** Results from Rahman et al. (Rahman et al., 2010) and the current model are compared, showing how \bar{Nu} varies with Ri for $Ha = 10$, $Pr = 0.71$, $Re = 100$.

$$e = \left| \frac{Nu_p - Nu_e}{Nu_e} \right| \times 100\% \quad (20)$$

where, Nu_p and Nu_e denote the Nusselt numbers obtained from the present simulation and existing literature, respectively. The calculated errors are 0.596 % for counter-clockwise rotation and 0.417 % for clockwise rotation when compared to the results of Mahmud et al. (Mahmud et al., 2022), and 0.375 % when compared to Rahman et al. (Rahman et al., 2010), who accounted for magnetohydrodynamic (MHD) effects. All errors fall well within the widely accepted threshold of 1 % for numerical simulations in convective heat transfer, thereby confirming the accuracy and reliability of the proposed model.

Fig. 5 shows that the results are quite accurate when comparing the two datasets, which in turn increases confidence in making computations via the model for various parameters.

5. Results and discussion

After performing the grid refinement analysis and validating the present model, a parametric study was carried out. During these simulations, several physical and governing parameters were held constant: $Ha = 10$, $k_s/k_f = 24.43$, $Pr = 5.85$, and the ratio of diameter to length (d/L) = 0.2. The range of governing parameters is summarized in Table 5 for three different case studies provided below. Consequently, a qualitative as well as a quantitative assessment of the behavior of the presented system was carried out. Key analyses focused on:

- Investigation of the distribution of the average Nusselt number and normalized Nusselt number on the heated bottom edge.
- The investigation of changes in the drag coefficient due to the sliding edge of the chamber.
- Comparison of the effect of internal heat generation or absorption within the enclosure with the cases without internal heat sources.

These results were calculated using equation (18) and are presented for each specific case. Furthermore, to comprehensively examine the effects of various mixed convection parameters, contour plots of temperature as well as stream function were systematically generated for each set of parametric modifications. These visualizations provided qualitative insights into the flow and thermal field behaviors. In the present numerical framework, the Richardson number (Ri) serves as the

Table 5

Description of the non-dimensional governing parameters for the current study:

Case	Ri	Gr	Re	Re_c	Δ
1	0.1–10	10^3 – 10^5	100	2, 0, -2	10, 0, -10
2	0.1–10	10^4	31.623–316.23	2, 0, -2	10, 0, -10
3	1	10^3 – 10^5	31.623–316.23	2, 0, -2	10, 0, -10

key indicator of the relative influence of buoyancy to inertial forces. Flows with $Ri < 0.1$ are classified as forced convection dominated, while $Ri > 10$ denotes natural convection dominated conditions where buoyancy prevails. The intermediate range, $0.1 \leq Ri \leq 10$, defines the mixed convection regime, where both buoyancy and inertia significantly influence flow behavior. The current study focuses on this mixed regime, with trends shifting toward forced or natural dominance at the lower and upper bounds of the Ri range, respectively. Initially, the streamlines and isotherms are visualized for carefully chosen combinations of Ri , Gr , Re , and Re_c .

5.1. Qualitative finding

5.1.1. Visualization of the flow field

Fig. 6 depicts the simplified patterns entrained within a lid-driven right-angled triangular enclosure housing a rotating cylinder. The flow field is influenced by Richardson number, Grashof number, and Reynolds number for streamlines drawn for both rotational directions of the cylinder: counterclockwise ($Re_c = -2$, black) and clockwise ($Re_c = 2$, blue). These visualizations illuminate the shape of internal flow structures as defined by the combined effects of forced convection (lid movement), natural convection (due to temperature gradients), and the cylinder rotation direction.

When $Ri = 0.1$ and $Gr = 10^4$ and a very high $Re = 316.23$, forced convection dominates the processes. The lid-driven shear generates strong circulation near the bottom-right corner, producing two main

eddies: one in the top part and another one almost at the bottom left of the space. Eddy shape and position depend on cylinder rotation. Counterclockwise rotation is depicted at $Re_c = -2$ in which the lower eddy rises, strengthening the flow disturbances close to the cylinder. On the other hand, $Re_c = 2$, shown by the clockwise rotation, is in the same direction as the main flow, which boosts the lower eddy and increases the rate of bottom mixing.

When Ri is raised to 1, the flow achieves the condition where both natural and forced convection impacts on the flow are nearly equal. This creates vortices at the top boundary where the thermal gradient and movement of the lid force the fluid up. With a further increase in Richardson number ($Gr = 10^4$, $Ri = 10$), the flow enters the natural convection-dominated regime where the role of buoyancy force becomes stronger. The upper vortex primarily expands and allows more air circulation across the cavity, further complicating the situation by cylinder rotation.

For moderate Reynolds and Grashof numbers ($Re = 100$, $Gr = 10^3$) and low Richardson ($Ri = 0.1$), the combination of inertial and buoyant forces causes relatively compact and stable eddy structures. With the increase of the Richardson number, buoyancy effects become more significant and induce shear induced instabilities, producing new eddies and a more widely distributed and complex flow field. The rotation of the cylinder slightly modifies the streamline displacements, aligning the streamlines with the cavity flow to either enhance or counter the circulation.

The internal flow structure and eddy dynamic are shaped by the cylinder's rotation direction and the interaction of Gr , Ri , and Re numbers and produce optimum heat transfer and temperature distribution. Buoyancy-driven natural convection, inertial forced convection, and controlled rotational effects result in a versatile thermal control mechanism within the enclosure, with an emphasis on regulating flow separation and enhancing thermal performance. The synergy between lid-driven flow and internal heat absorption highlights opportunities in thermal management for high-power electronics, where high Re and low

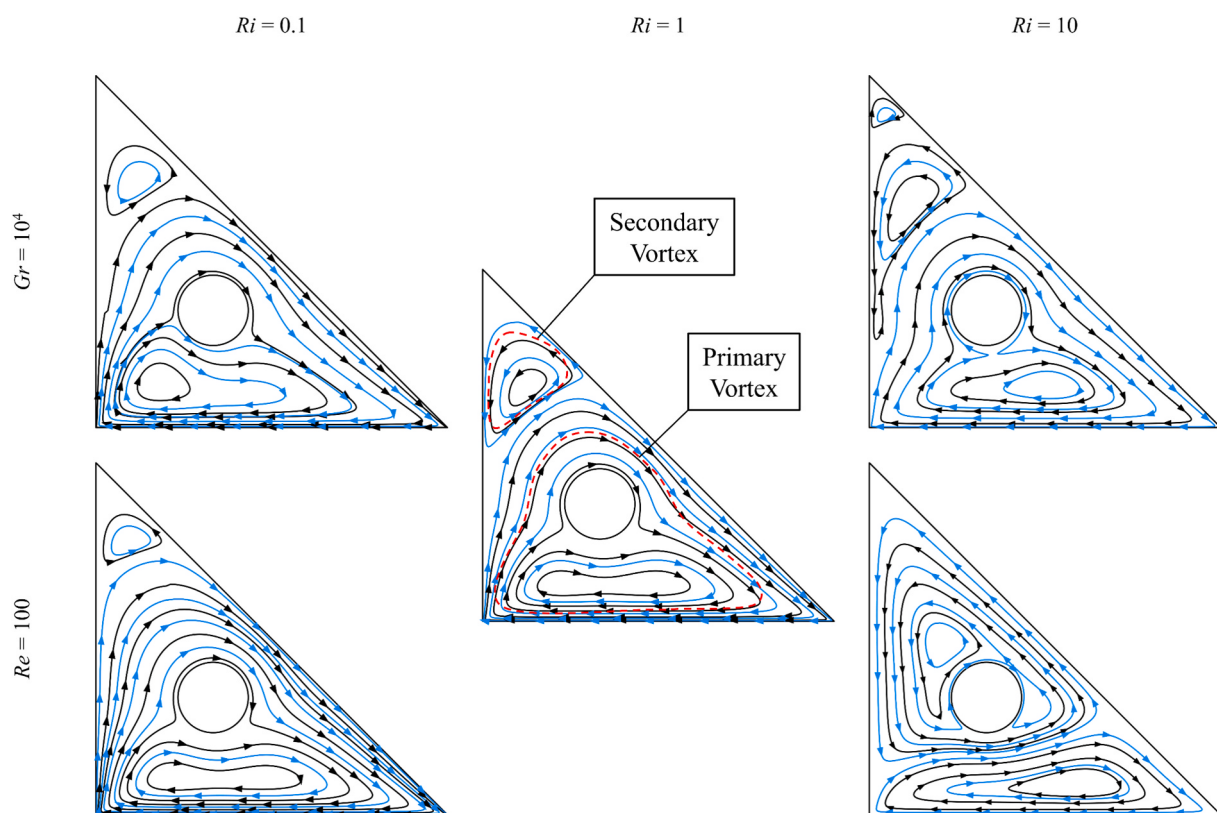


Fig. 6. Streamline pattern visualization for different Ri , Gr , and Re at $\Delta = -10$. The black and blue lines indicate $Re_c = -2$ and $Re_c = 2$ streamlines, respectively.

Ri promote uniform heat distribution. Optimizing lid velocity and employing heat-absorbing fluids can enhance cooling in compact heat sinks. Moreover, the magnetic field's ability to suppress recirculation zones can be leveraged to improve flow uniformity in heat exchangers, enhancing mixing and thermal recovery in industrial systems.

5.1.2. Visualization of the thermal field

Fig. 7 shows the isotherm patterns in a lid-driven right-angled triangular enclosure with a rotating cylinder at the center for different Richardson (Ri), Grashof (Gr), and Reynolds (Re) numbers, illustrating how the temperature field is affected. A color scale from blue to red represents a temperature gradient, with red corresponding to areas of higher temperature near heated surfaces and blue adjacent to cold boundaries.

In a high Reynolds number ($Re = 316.23$) regime and a low Richardson number ($Ri = 0.1$) with $Gr = 10^4$, the forced convection effect is prominent because of the contribution of lid-driven flow. Hot fluid pushed up from the heated surface by the fast-moving bottom lid wraps around the rotating cylinder and mixes with the cooler fluid along the cooled vertical wall. The high-temperature fluid is effectively distributed through the enclosure by this forced flow, resulting in a more uniform temperature field surrounding the cylinder. The emphasis in this scenario is on the strong influence of forced convection due to the combined moving lid and heated surface, which leads to a broad and uniform distribution of heat.

When the Richardson number increases to $Ri = 1$, there will be transitional values between forced and natural convection. The buoyancy effects become relatively important when Gr is still at 10^4 and hot fluid starts to move upward by the natural convection. Nevertheless, a degree of mixing is still indicated by the forced flow in the moving lid. The resulting temperature distribution for this mixed convection regime is somewhat less uniform than at $Ri = 0.1$ but still shows pronounced heat spread around the cylinder. The isotherm patterns indicate an intermediate behavior, in which buoyancy and lid-driven flow make a

significant contribution to the heat transfer process.

At $Gr = 10^4$, when the Richardson number reaches its maximum value ($Ri = 10$), natural convection will dominate the buoyancy forces. The hot fluid rises naturally, and here we distinguish a well-formed thermal plume near the bottom of the enclosure and more dispersion around the cylinder. In this case, the isotherms present heat concentration around the hot wall, but cooler regions settle around the cold vertical boundary. The absence of strong forced flow predicts a less efficient heat transfer across the enclosure, reducing the mixing of hot and cold fluids.

For $Re = 100$, and increasing Gr from 10^3 to 10^5 the buoyancy forces were determined to be stronger and the natural convection was observed to be more affected. The circulation patterns are vigorous in this configuration as thermal plumes form within the enclosure. Prominent thermal circulation is caused by natural convection, but it does not produce the same level of uniform temperature distribution as forced mixed convection. The presence of the high buoyancy forces makes it accumulate the heat near the hot wall, generating some localized hot zones that limit the heat transfer efficiency across the enclosure.

Results indicate that a balance between forced and natural convection ($Ri = 1$) gives moderate thermal uniformity. However, forced convection (low Ri) is more effective at spreading the heat, at least over a wider extent when a sufficiently high Reynolds number provides enough mixing. It is demonstrated that thermal field distribution can be controlled by adjusting parameters like Ri , Gr , and Re , and this is important for thermal enclosures, solar collectors, and even energy-efficient building design. High Ri values lead to localized hot zones that can reduce efficiency in applications like solar thermal collectors. However, combining moderate lid motion ($Re = 100$) with internal heat absorption ($\Delta = -10$) helps stabilize temperature gradients. Additionally, the negligible effect of cylinder rotation suggests that simpler, stationary designs may be sufficient for rotating machinery, lowering maintenance without compromising thermal performance.

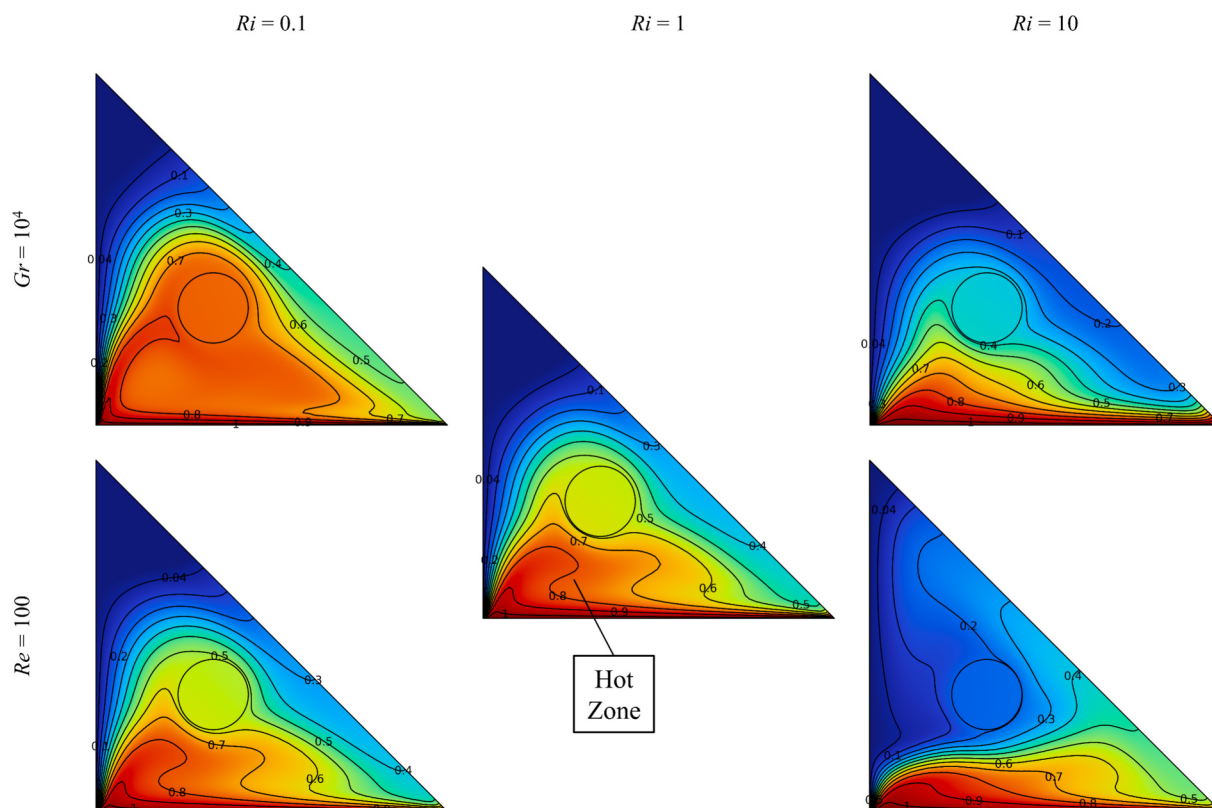


Fig. 7. Isotherm pattern visualization for different Ri , Gr , and Re at $\Delta = -10$ and $Re_c = -2$.

5.2. Quantitative analysis

5.2.1. Distribution of average Nusselt number

The average Nusselt numbers for Case 1 are shown in Fig. 8, demonstrating a quantitative representation of the impact of different factors on the average Nusselt numbers. In particular, Fig. 8(a) illustrates a comparison of the thermal behavior of a lid-driven, right-angled triangular enclosure containing a rotating cylinder at various Richardson (Ri) and Grashof (Gr) number values. According to the present data, the average Nusselt number holds a relatively constant value at forced convection-dominated conditions that imply heat transfer due to uniform sliding movement of the bottom wall of the enclosure. Thus, in these regimes, the rotation direction of the cylinder, whether clockwise, counterclockwise, or stationary, does not significantly affect heat transfer augmentation. This makes it to imply that heat transportation is mainly caused by the forced convection from the moving wall rather than the rotation of the cylinders. With the increase in Ri , associated with the transition to the free convection dominant regime, the Nusselt number gradually decreases, with a sharp decline observed from approximately $Ri = 1$ at $Gr = 10^4$. In this regime, buoyancy effects increase with heated fluid accumulating beneath the hot bottom surface in a manner that adversely affects the flow and limits convection. Overall, the results suggest that heat transfer is predominantly governed by Ri and Gr , while the role of cylinder rotation remains secondary across both forced and free convection regimes.

Fig. 8(b) illustrates the thermal performance variations within a lid-driven triangular enclosure under different internal heat conditions: The heat generation and absorption are, respectively, $\Delta = 10$ and $\Delta = -10$, and there is no internal heat source or sink, $\Delta = 0$. Figures show the relationship between forced and natural convection by investigating the average Nusselt number (Nu) as a function of the Richardson (Ri) and Grashof (Gr) numbers. In the forced convection, the Nusselt number does not vary much among all cases, but unique behaviors prevail at high regimes. The reason simply comes down to the fact that the sliding bottom wall minimizes internal heat effects in the forced convection domain. However, analyzing the overall scenario, the Nusselt number, or heat transfer enhancement, occurs when $\Delta = -10$ (heat is being absorbed), that is, for a steeper temperature gradient to transport the heat. On the other hand, when $\Delta = 10$ (heat generation), the Nusselt number becomes the lowest. Here convective efficiency is disrupted by internal heat generation, although buoyancy gives a slight improvement at larger Ri . Between these two extremes, the case where $\Delta = 0$ (no internal heat source or sink) reveals a case of moderate heat transfer affected by both sliding and buoyancy.

The distribution of the average Nusselt number for Case 2 is

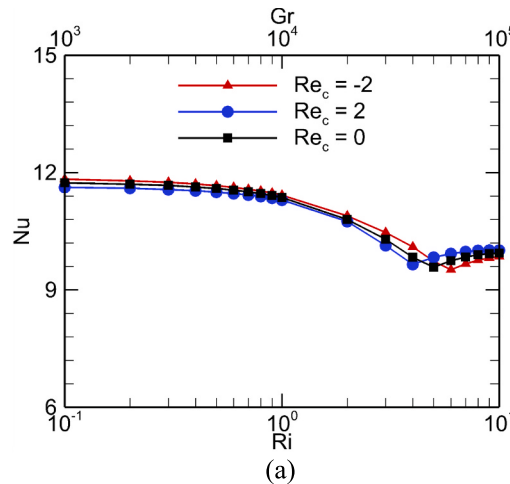


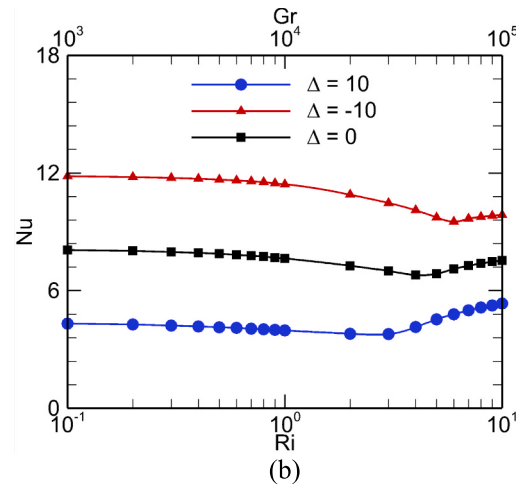
Fig. 8. Values of (a) Re_c (2, 0, -2) at $\Delta = -10$ and (b) Δ (10, 0, -10) at $Re_c = -2$ are observed for Nu as a function of Gr and Ri numbers (Case 1).

presented in Fig. 9 to quantify the effect of various governing parameters. In Fig. 9(a), the average Nusselt number decreases as the Reynolds number decreases, implying a fall in heat transfer. This trend is analogous to the decrease in fluid circulation resulting from the reduced velocity of the bottom lid driven wall and hence the reduction of the convective heat transfer from the heated bottom surface to the cooler regions in the enclosure. With increasing Ri compared to Re , the transition occurs from forced convection dominated regime to a mixed convection regime where a reduction in Nu is due to increasing contribution of buoyancy driven natural convection. Across all cases, cylinder rotation (Re_c) exerts only a marginal influence on Nu , underscoring the dominant role of lid-driven motion in determining convective performance.

The average Nusselt number at the heated bottom moving wall of the enclosure decreases as the values of Ri and Re increase, respectively, as shown in Fig. 9(b). The Nusselt number decreases for all cases as Ri rises, signifying a shift toward natural convection and a decrease in convective heat transfer as a result of lower fluid velocities. This transition to natural convection inhibits mixing at the hot and cold regions, thus reducing the temperature gradient at the heated wall, leading to a poorer heat transfer efficiency. Internal heat conditions also have an effect: with internal heat sources ($\Delta = 10$), heat transfer is suppressed even more due to the increased fluid temperature, which leads to the thickening of the thermal boundary layer, a reduced temperature gradient at the wall, and consequently the lowest Nusselt numbers. Conversely, internal heat absorption ($\Delta = -10$) can improve heat transfer by reducing the fluid temperature, allowing a higher thermal gradient to be maintained and consequently higher Nusselt numbers, particularly in the convection dominant regimes. The graph thus highlights how both natural convection dominance (high Ri) and internal heat generation can reduce heat transfer efficiency, while heat absorption improves it by sustaining larger temperature differences at the heated wall.

Fig. 10(a) shows the dependence of the average Nusselt number (Nu), Grashof number (Gr), and Reynolds number (Re) on cylinder angular velocities ($Re_c = -2, 0, 2$) as well as a fixed Richardson number (Ri). Results reveal that Nu rises dramatically as Gr and Re rise, implying that the heat transfer is enhanced by convective flows intensified by buoyancy and lid motion. The curves for different Re_c values overlap closely, indicating that cylinder rotation plays only a minor role. It implies that the effects of buoyancy and forced convection are dominant, with rotational disturbances becoming negligible under stronger convection.

Fig. 10(b) illustrates the impact of Re and Gr numbers in a specific scenario at $Ri = 1$, which denotes pure mixed convection. By raising the



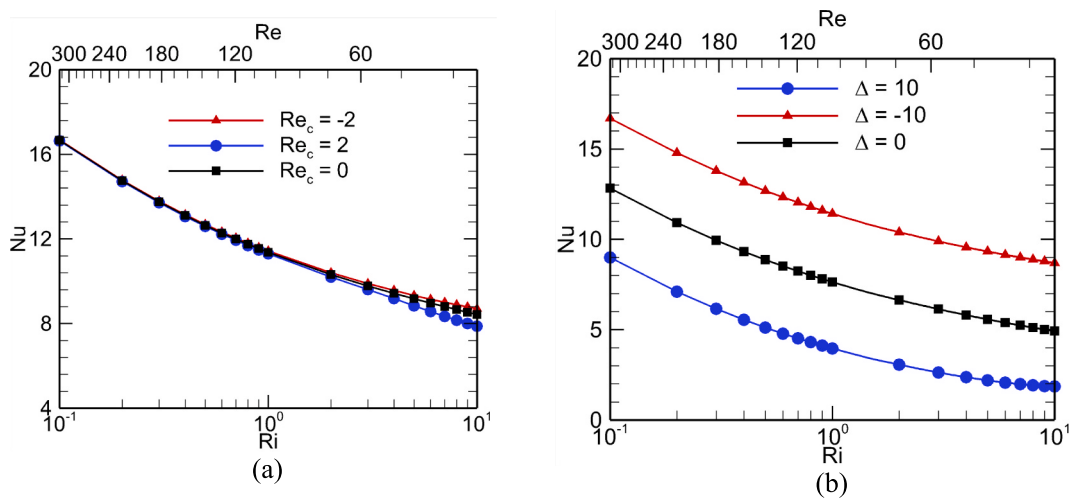


Fig. 9. Values of (a) Re_c (2, 0, -2) at $\Delta = -10$ and (b) Δ (10, 0, -10) at $Re_c = -2$ are observed for Nu as a function of Re and Ri numbers (Case 2).

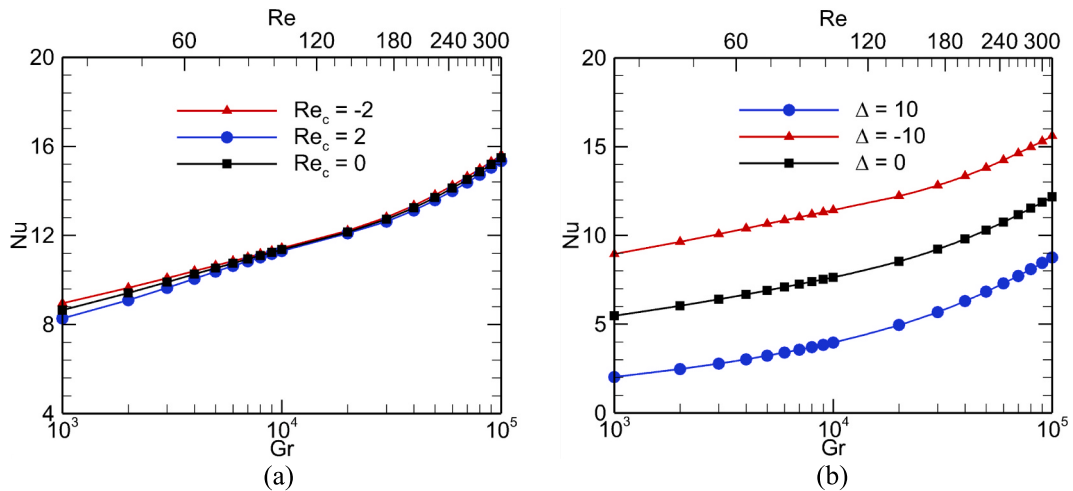


Fig. 10. Values of (a) Re_c (2, 0, -2) at $\Delta = -10$ and (b) Δ (10, 0, -10) at $Re_c = -2$ are observed for Nu as a function of Gr and Re numbers (Case 3).

Nusselt number as the Grashof and Reynolds numbers rise, the data show that buoyancy-driven flow and lid-driven shear boost heat transfer inside the enclosure at Δ (10, 0, -10). The maximum value of Nu is obtained at $\Delta = -10$, and this reveals that internal heat absorption raises the temperature gradient and strengthens the convection, which in turn enhances heat transfer. On the other hand, the value of Nu is smaller at $\Delta = 10$, which means that convection heat transmission is happening relatively less, and internal heat generation influences the temperature gradient. A baseline of comparison is represented by the $\Delta = 0$ curve, which corresponds to no internal heat generation or absorption. For the most part, the graph shows that increasing Gr and Re , by increasing the difference of the temperature across the enclosure and the sliding speed of the lid, increases heat transfer greatly.

5.2.2. Distribution of normalized Nusselt Number

Fig. 11 shows how normalized Nusselt numbers vary with the dimensionless numbers Re , Ri , and Gr in the triangular cavity for different Re_c . Although Fig. 8(a), 9(a), and 10(a) expose minor variability with respect to changes in Re_c , Fig. 11 shows more complex variations.

Fig. 11(a) shows the variation in Nu_{nor} with Ri and Gr at $Re_c = \pm 2$. With low Ri , signifying forced convection, Nu_{nor} is observed close to unity, indicating that heat transfer is almost entirely due to forced convection by lid-driven motion. However, when it transitions to that of

high Ri , the flow is more tilted toward free convection, and then heat transfer starts to diverge for both rotation direction cases. Clockwise rotation ($Re_c = -2$) reduces the Nu_{nor} value below unity, indicating suppression of heat transfer since it creates local circulations due to counteracting influences between cylinder rotation and buoyancy-induced natural convection. Conversely, the counterclockwise rotation ($Re_c = 2$) improves heat transfer and increases Nu_{nor} greater than unity at higher Ri . This improvement is due to the synergistic interaction between cylinder rotation and natural convection leading to better thermal mixing. In addition, the importance of cylinder rotation decreases as Ri is increased further, with thermal stratification becoming more dominant. These trends result from the interplay between buoyancy and rotational dynamics and are shown to be sensitive to those parameters.

Fig. 11(b) depicts Nu_{nor} as a function of Re and Ri at fixed Gr for both rotation directions. The thermal regime then shifts from forced to a natural convection regime when Re decreases and Ri increases. Under such conditions, clockwise rotation ($Re_c = -2$) slightly improves heat transfer with Nu_{nor} values above unity. This enhancement of heat transfer is caused by the rotating cylinder alignment between the buoyancy-driven flow, which promotes the mixing of fluids and causes upward movement of heat. However, counterclockwise rotation ($Re_c = 2$) reduces the heat transfer with Nu_{nor} values below unity. By disrupting the natural flow structure, the counter-rotating cylinder generates localized vortices that impair heat transport efficiency. These

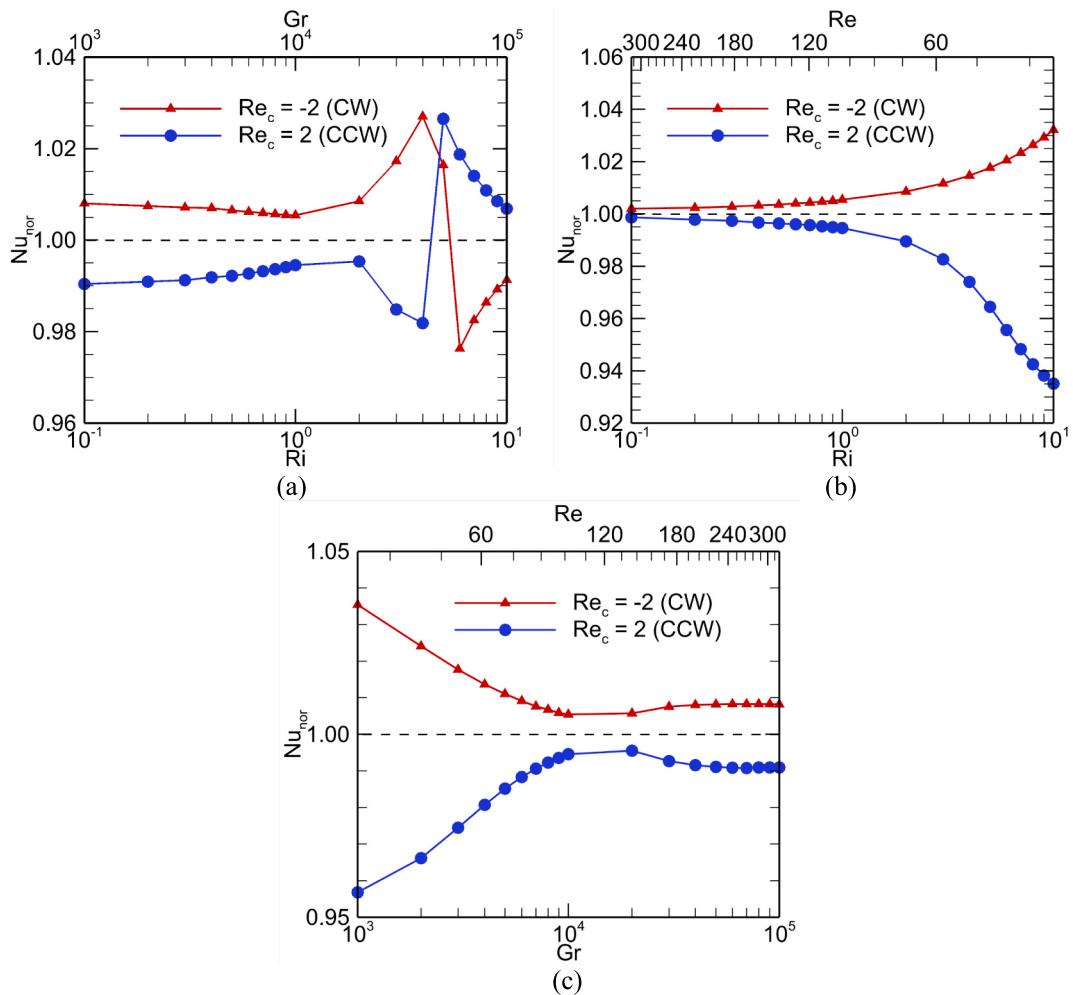


Fig. 11. Observation of the normalized Nusselt number as a function of Re_c (-2, 2) at $\Delta = -10$ for distinct values of (a) Ri and Gr (case 1), (b) Ri and Re (case 2), and (c) Gr and Re (case 3).

observations highlight the complex effect of cylinder rotation on convection which indicate that buoyancy effects can be enhanced with clockwise rotation to promote thermal performance, especially in natural convection regimes, while counterclockwise rotation imposes a competing influence that reduces thermal efficiency.

Nu_{nor} as a function of Gr and Re for both rotation directions at a fixed

Ri is depicted in Fig. 11(c). At low Re and Gr , the clockwise rotation ($Re_c = -2$) significantly enhances fluid mixing and heat transfer. This is a result of a synergistic alignment between buoyancy-driven flow and rotational motion to produce effective thermal mixing. On the other hand, counterclockwise rotation ($Re_c = 2$) creates a circulation zone in the top corner of the cavity, decreasing natural convective flow and

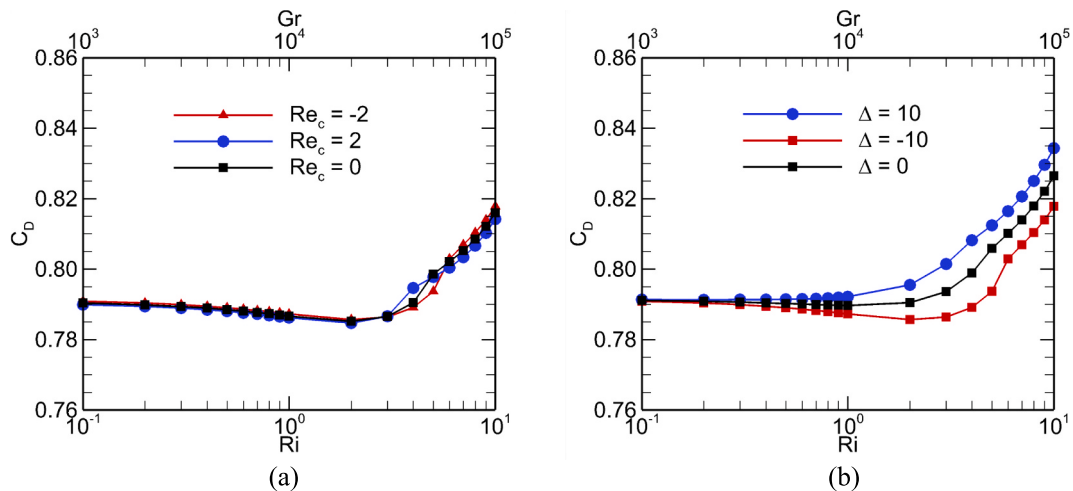


Fig. 12. Changes in C_d on a sliding lid as a function of Ri and Gr (Case 1) over a range of values of (a) Re_c (2, 0, -2) at $\Delta = -10$ and (b) Δ (10, 0, -10) at $Re_c = -2$.

reducing overall heat transfer efficiency. The impact of the rotation of the cylinder tends to decrease when the values of Re or Gr are increased where inertial forces dominate in that instance.

5.2.3. Distribution of average drag coefficient

Fig. 12(a) presents the variation of the average drag coefficient (C_d) on the moving lid of a lid-driven triangular enclosure as a function of Richardson (Ri) and Grashof numbers (Gr) for different rotational Reynolds numbers (Re_c) of the cylinder at a fixed Reynolds number ($Re = 100$). The forced convection dominated regime (inertial forces > buoyancy) shows nearly constant Drag Coefficient (C_d), due to the formation of stable compact eddy structures independent of cylinder rotation. However, as Ri and Gr increase, the buoyancy forces become more pronounced, and additional eddies start developing within the cavity, forming much more complicated flow patterns, as discussed in **Fig. 6**. This change in flow structure results in a higher C_d value since increased fluid circulation produces bigger and a more widespread distribution of eddies within the natural convection-dominated regime.

Fig. 12(b) shows the average drag coefficient of the sliding enclosure lid having different values of Gr and Ri for different heat generation/absorption coefficients at a fixed Re . In the forced convection-dominated regime, the internal heat generation or absorption has a negligible effect on C_d , as the motion given by the lid drives the fluid, thus attenuating the buoyancy effect. With the increase, Ri directs the flow towards natural convection with an increased effect of Δ . Heat generation ($\Delta =$

10) produces the highest C_d in natural convection dominated flow because buoyancy forces increase motion at the heated lid, elevating the velocity gradient and consequently C_d . On the other hand, heat absorption, ($\Delta = -10$), results in the lowest C_d because a lower temperature gradient decreases buoyancy forces, resulting in lower fluid velocities close to the lid. The neutral case ($\Delta = 0$) would therefore show commensurate intermediate values of C_d . Further, it was observed that these effects are augmented with increasing Grashof number, and the difference in C_d between the two cases is significant at high Ri , particularly at $Gr = 10^5$.

Average drag coefficients (C_d) for a sliding lid of the driven lid right-angle triangular enclosure are presented in **Fig. 13(a)** and **13(b)** as functions of Richardson (Ri) and Reynolds (Re) numbers. The figures show how cylinder rotation speed and internal heat generation or absorption affect the drag coefficient. In both the figures, C_d increases with increasing values of Ri , as the flow regime changes from forced convection (lower Ri) to natural convection (higher Ri).

Fig. 13(a) shows that the effects of cylinder rotation speed ($Re_c = -2, 0, 2$) on C_d are insignificant as Ri varies. This indicates that under this condition, the lid's motion dominates the drag force, with the cylinder rotation having little effect on the flow field. Additionally, **Fig. 13(b)** portrays the influences of internal heat generation and absorption (with $\Delta = 10, 0, -10$) on C_d while Re_c is held at -2 . At lower Ri values, the C_d is not very sensitive to the changes in Δ . However, as Ri increases, some fluctuations in C_d are noted when internal heat generation or absorption

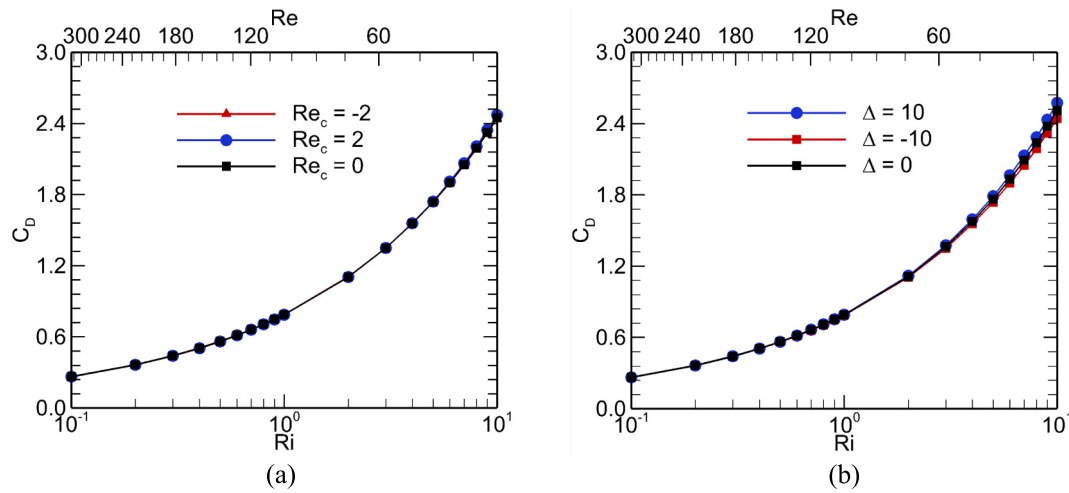


Fig. 13. Changes in C_d on a sliding lid as a function of Re and Ri (Case 2) over a range of values of (a) Re_c (2, 0, -2) at $\Delta = -10$ and (b) Δ (10, 0, -10) at $Re_c = -2$.

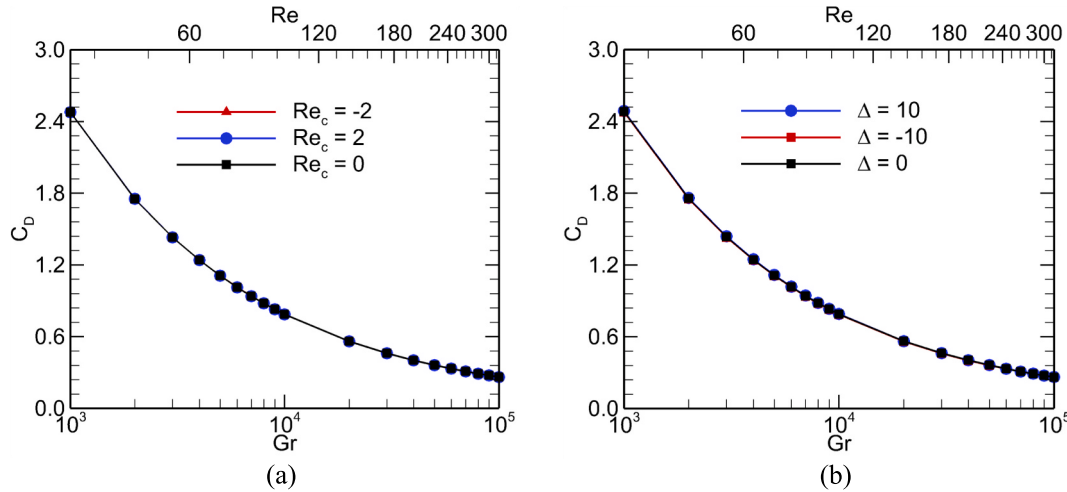


Fig. 14. Changes in C_d on a sliding lid as a function of Gr and Re (Case 3) over a range of values of (a) Re_c (2, 0, -2) at $\Delta = -10$ and (b) Δ (10, 0, -10) at $Re_c = -2$.

Table 6Summary of key outcomes for various Re and Gr at $\Delta = -10$ and $Re_c = -2$:

Re	Gr	Nu	C_d	Nu_{hor}
31.623	10^3	8.946	2.476	1.035
100	10^4	11.423	0.787	1.005
316.23	10^5	15.604	0.262	1.008

exists. This data indicates that although enhancement or reduction in internal heat generation or absorption leads to minor modification in buoyancy-driven flow, it does not considerably affect the drag coefficient around the moving lid.

As seen in Fig. 14(a) and 14(b), the average drag coefficient (C_d) on the moving lid of a right-angled triangular enclosure decreases with increasing Grashof number (Gr) and Reynolds number (Re). Regardless of the variations in cylinder rotational speed ($Re_c = -2, 0, 2$) or internal heat generation/absorption ($\Delta = 10, 0, -10$), the trend is the same. This gives rise to an increased Gr that aids in increasing buoyancy forces and a higher Re , which leads to faster lid movement, increasing fluid circulation and resulting in lower resistance of the lid. Temperature distribution and flow characteristics have been modified due to different internal generation/absorption and rotational speeds, but quite insignificantly in comparison to their effects on C_d concerning Gr and Re . The uniform decreases in C_d across different cases indicate that in mixed convection with $Ri = 1$, the interaction between buoyant and inertial forces dominates drag reduction while the rotational effects and internal heat generation are secondary. The enhanced heat transfer efficacy is evident from this behavior, resulting from the increased fluid motion in this enclosure.

The Table 6 summarizes the parameters and outcomes for pure mixed convection scenario (Case 3):

6. Conclusion

This study conducts a rigorous numerical investigation of conjugate mixed convection coupled with magnetohydrodynamic effects in a right-angled triangular enclosure filled with a swirling reactive fluid and incorporating a rotating, heat-conducting cylinder. The computational model was numerically discretized and solved, enabling an exploration of the impact of Δ , Re_c , Ri , Gr , and Re on flow and heat transfer patterns.

The principal findings of this research are as follows:

1. Enhanced Heat Transfer

Heat transfer in the enclosure was significantly enhanced by the combined effects of lid motion, thermal gradients, and internal heat absorption. At the highest Reynolds number ($Re = 316.23$) and Grashof number ($Gr = 10^5$), internal heat absorption increased the average Nusselt number by up to 74.5 %, clearly demonstrating the strong synergistic interaction of these mechanisms in boosting thermal performance.

2. Effect of Lid Velocity on Drag and Heat Transfer

Increasing lid velocity intensified flow circulation, enhancing heat transfer while reducing the drag coefficient by up to 89 % under internal heat absorption. This reveals that higher speeds can simultaneously improve thermal efficiency and reduce mechanical resistance.

3. Importance of Thermal Gradient and Lid Velocity on Heat Transfer

Maximum heat transfer occurred when both Grashof and Reynolds numbers were high. The thermal gradient drove buoyancy forces, while lid velocity added forced convection, and their combination resulted in optimal convective performance, highlighting their synergistic role.

4. Role of Internal Heat Absorption for Temperature Uniformity

Internal heat absorption acted as a volumetric heat sink, smoothing temperature gradients and promoting uniform temperature distribution. This stabilization of the thermal field improved convective effectiveness and reduced local thermal hotspots.

5. Marginal Impact of Cylinder Rotation

Rotating the central solid cylinder had a minor effect on flow and thermal performance, with only slight changes in streamlines, isotherms, and average Nusselt number. Lid motion and internal heat effects remained the dominant influences.

These findings contribute to a deeper understanding of the complex dynamics involved in mixed convection systems under the influence of magnetic fields and internal heat generation. The insights gained from this study offer valuable guidance for the thermal design and optimization of systems such as chemical reactors, heat exchangers, and solar thermal collectors, where precise control of heat transfer, flow behavior, and rotational components under magnetic and internal heat effects is essential.

Limitations and Future Work

While this study provides critical insights, it assumes 2D laminar flow and idealizes geometry/boundary conditions (fixed wall temperatures, uniform magnetic field). Future work should:

1. Extend to 3D transient simulations and incorporate turbulence models to better capture high- Re dynamics.
2. Evaluate systems with non-Newtonian fluids and realistic geometries or time-dependent boundary conditions.
3. Incorporate thermal radiation and Joule heating effects, especially in MHD-dominated regimes.
4. Apply findings in system-level simulations for advanced design of solar collectors, reactors, and heat exchangers.

Declaration of competing interest

The authors declare that they have no known competing financial interests or personal relationships that could have appeared to influence the work reported in this paper.

Data availability

Data will be made available on request.

References

- Ali, M.M., Akhter, R., Alim, M.A., 2022. Magneto-mixed convection in a lid driven partially heated cavity equipped with nanofluid and rotating flat plate. Alex. Eng. J. 61 (1), 257–278. <https://doi.org/10.1016/j.aej.2021.05.003>.
- Selimefendigil, F., Öztop, H.F., 2017. Mixed convection in a partially heated triangular cavity filled with nanofluid having a partially flexible wall and internal heat generation. J. Taiwan Inst. Chem. Eng. 70, 168–178. <https://doi.org/10.1016/j.jtice.2016.10.038>.
- Chamkha, A.J., Selimefendigil, F., Oztop, H.F., 2018. MHD mixed convection and entropy generation in a lid-driven triangular cavity for various electrical conductivity models. Entropy 20 (12). <https://doi.org/10.3390/e20120903>.
- Shahid, H., Yaqoob, I., Khan, W.A., Rafique, A., 2021. Mixed convection in an isosceles right triangular lid driven cavity using multi relaxation time lattice Boltzmann method. Int. Commun. Heat Mass Transfer 128. <https://doi.org/10.1016/j.icheatmasstransfer.2021.105552>.
- Uddin, M.N., Farhana, A., Alim, A., 2015. Finite element analysis of magneto-hydrodynamic (Mhd) mixed convection flow in a lid-driven triangular cavity. J. Nav. Archit. Mar. Eng. 12 (1), 21–32. <https://doi.org/10.3329/jname.v12i1.12910>.
- Selimefendigil, F., Öztop, H.F., Chamkha, A.J., 2016. MHD mixed convection and entropy generation of nanofluid filled lid driven cavity under the influence of inclined magnetic fields imposed to its upper and lower diagonal triangular domains. J. Magn. Magn. Mater. 406, 266–281. <https://doi.org/10.1016/j.jmmm.2016.01.039>.
- Çolak, E., Öztop, H.F., Ekici, Ö., 2020. MHD mixed convection in a chamfered lid-driven cavity with partial heating. Int. J. Heat Mass Transf. 156. <https://doi.org/10.1016/j.ijheatmasstransfer.2020.119901>.

- Oztop, H.F., Al-Salem, K., Pop, I., 2011. MHD mixed convection in a lid-driven cavity with corner heater. *Int. J. Heat Mass Transf.* 54 (15–16), 3494–3504. <https://doi.org/10.1016/j.ijheatmasstransfer.2011.03.036>.
- Al-Salem, K., Öztop, H.F., Pop, I., Varol, Y., 2012. Effects of moving lid direction on MHD mixed convection in a linearly heated cavity. *Int. J. Heat Mass Transf.* 55 (4), 1103–1112. <https://doi.org/10.1016/j.ijheatmasstransfer.2011.09.062>.
- Khanafer, K., Aithal, S.M., 2013. Laminar mixed convection flow and heat transfer characteristics in a lid driven cavity with a circular cylinder. *Int. J. Heat Mass Transf.* 66, 200–209. <https://doi.org/10.1016/j.ijheatmasstransfer.2013.07.023>.
- Haq, R.U., Soomro, F.A., Wang, X., Tili, I., 2020. Partially heated lid-driven flow in a hexagonal cavity with inner circular obstacle via FEM. *Int. Commun. Heat Mass Transfer* 117. <https://doi.org/10.1016/j.icheatmasstransfer.2020.104732>.
- Soomro, F.A., Haq, R.U., Alghayne, E.A., Tili, I., 2020. Thermal performance due to magnetohydrodynamics mixed convection flow in a triangular cavity with circular obstacle. *J. Energy Storage* 31. <https://doi.org/10.1016/j.est.2020.101702>.
- Xiong, P.Y., Hamid, A., Iqbal, K., Irfan, M., Khan, M., 2021. Numerical simulation of mixed convection flow and heat transfer in the lid-driven triangular cavity with different obstacle configurations. *Int. Commun. Heat Mass Transfer* 123. <https://doi.org/10.1016/j.icheatmasstransfer.2021.105202>.
- O. Younis, S. E. Ahmed, A. Abderrahmane, A. Alenazi, and A. M. Hassan, "Hydrothermal Mixed Convection in a Split-Lid-Driven Triangular Cavity Suspended by NEPCM," *Mathematics*, vol. 11, no. 6, Mar. 2023, doi: 10.3390/math11061323.
- Hussain, Z., Alghamdi, M., Fozia, S., Ali, M.R., Ali, and M. Aslam., 2023. Significance of mixed convective heat transfer model in an equilateral triangular enclosure subjected to cylindrical heated objects inside. *Case Stud. Therm. Eng.* 47. <https://doi.org/10.1016/j.csite.2023.103027>.
- Costa, V.A.F., Raimundo, A.M., 2010. Steady mixed convection in a differentially heated square enclosure with an active rotating circular cylinder. *Int. J. Heat Mass Transf.* 53 (5–6), 1208–1219. <https://doi.org/10.1016/j.ijheatmasstransfer.2009.10.007>.
- Liao, C.C., Lin, C.A., 2014. Mixed convection of a heated rotating cylinder in a square enclosure. *Int. J. Heat Mass Transf.* 72, 9–22. <https://doi.org/10.1016/j.ijheatmasstransfer.2013.12.081>.
- Mamun, M.A.H., Prince, H.A., Siam, M.M.H., 2023. Variations of MHD double-diffusive mixed convection and entropy generation in various nanofluids and hybrid nanofluids due to the deviation of the spinning of double rotating cylinders. *International Journal of Thermofluids* 20. <https://doi.org/10.1016/j.ijft.2023.100421>.
- Selimefendigil, F., Oztop, H.F., Chamkha, A.J., 2019. Analysis of mixed convection and entropy generation of nanofluid filled triangular enclosure with a flexible sidewall under the influence of a rotating cylinder. *J. Therm. Anal. Calorim.* 135 (2), 911–923. <https://doi.org/10.1007/s10973-018-7317-5>.
- Aissa, A., Belazreg, A., Laidoudi, H., Mohammed, S., Younis, O., Alazzam, A., 2024. Enhanced heat transmission in a triangular enclosure with a rotating cooled wall using Nano-Encapsulated phase Change Material nanofluid under mixed convection. *Case Stud. Therm. Eng.* 54. <https://doi.org/10.1016/j.csite.2024.103992>.
- Amine, B.M., Redouane, F., Mourad, L., Jamshed, W., Eid, M.R., Al-Kouz, W., 2021. Magnetohydrodynamics Natural Convection of a Triangular Cavity Involving Ag-MgO/Water Hybrid Nanofluid and provided with Rotating Circular Barrier and a Quarter Circular Porous Medium at its Right-Angled Corner. *Arab. J. Sci. Eng.* 46 (12), 12573–12597. <https://doi.org/10.1007/s13369-021-06015-6>.
- A. N. M. F. Islam, R. Islam, S. Javed, and S. Saha, "Optimization of system parameters during conjugate mixed convective flow in a square domain with an oscillating spinning cylinder," *Heliyon*, vol. 10, no. 2, Jan. 2024, doi: 10.1016/j.heliyon.2024.e24258.
- Mahmud, M.J., Rais, A.I., Hossain, M.R., Saha, S., 2022. Conjugate mixed convection heat transfer with internal heat generation in a lid-driven enclosure with spinning solid cylinder. *Heliyon* 8 (12). <https://doi.org/10.1016/j.heliyon.2022.e11968>.
- Paul, D.K., Al Mehedi, A., Chowdhury, E.H., Saha, S., Ali, M., Ruhul Amin, M., 2021. Conjugate mixed Convection in a Differentially Heated Lid-Driven Square Cavity with Rotating Cylinders. ASME International Mechanical Engineering Congress and Exposition, Proceedings (IMECE) 11. <https://doi.org/10.1115/IMECE2020-23339>.
- Rasel, M.S., Rupam, M.T.I., Shuvo, M.S., Saha, S., 2023. Investigation on conjugate mixed convection through a vented chamber with heat generating and conducting rotating circular cylinders. *Results Eng.* 19. <https://doi.org/10.1016/j.rineng.2023.101248>.
- E. H. Chowdhury, A. Al Mehedi, D. K. Paul, S. Saha, and M. Ali, "Conjugate pure mixed convection in a differentially heated lid-driven square cavity with two rotating cylinders," in *AIP Conference Proceedings*, American Institute of Physics Inc., Feb. 2021. doi: 10.1063/5.0037523.
- Hasan, N., Saha, S., 2024. Effects of internal heat production and Joule heating on MHD conjugate mixed convection and entropy production inside a thermally non-homogeneous cooling system. *Ann. Nucl. Energy* 206. <https://doi.org/10.1016/j.anucene.2024.110671>.
- Chatterjee, D., Mondal, B., Halder, P., 2014. Hydromagnetic mixed convective transport in a vertical lid-driven cavity including a heat conducting rotating circular cylinder. *Numeri Heat Transf A Appl* 65 (1), 48–65. <https://doi.org/10.1080/10407782.2013.812399>.
- Javed, S., Saha, S., 2023. Estimation of comprehensive thermal performance for conjugate natural convection inside a dome-shaped porous chamber holding a solid cylinder. *Results Eng.* 17. <https://doi.org/10.1016/j.rineng.2023.100896>.
- Tasnim, S., Shuvo, M.S., Deb, N., Islam, M.S., Saha, S., 2023. Entropy generation on magnetohydrodynamic conjugate free convection with Joule heating of heat-generating liquid and solid element inside a chamber. *Case Stud. Therm. Eng.* 52. <https://doi.org/10.1016/j.csite.2023.103711>.
- Rahman, M.M., Alim, M.A., Sarker, M.M.A., 2010. Numerical study on the conjugate effect of joule heating and magneto-hydrodynamics mixed convection in an obstructed lid-driven square cavity. *Int. Commun. Heat Mass Transfer* 37 (5), 524–534. <https://doi.org/10.1016/j.icheatmasstransfer.2009.12.012>.
- Chamkha, A.J., 2002. Hydromagnetic combined convection flow in a vertical lid-driven cavity with internal heat generation or absorption. *Numeri Heat Transf A Appl* 41 (5), 529–546. <https://doi.org/10.1080/104077802753570356>.
- Sivasankaran, S., Sivakumar, V., Hussein, A.K., Prakash, P., 2014. Mixed convection in a lid-driven two-dimensional square cavity with corner heating and internal heat generation. *Numeri Heat Transf A Appl* 65 (3), 269–286. <https://doi.org/10.1080/10407782.2013.826017>.
- N. Hasan, S. Saha, and J. C. Umavathi, "Magnetohydrodynamic convection in a heat-generating ferrofluid within a corrugated cavity containing a rotating cylinder," *Physics of Fluids*, vol. 36, no. 7, Jul. 2024, doi: 10.1063/5.0216132.
- Saha, L.K., 2015. Effect of Internal Heat Generation or Absorption on MHD mixed Convection Flow in a Lid Driven Cavity. *American Journal of Applied Mathematics* 3 (1), 20. <https://doi.org/10.11648/j.ajam.s.2015030101.13>.
- Mahmoudi, A., Mejri, I., Abbassi, M.A., Omri, A., 2014. Analysis of the entropy generation in a nanofluid-filled cavity in the presence of magnetic field and uniform heat generation/absorption. *J. Mol. Liq.* 198, 63–77. <https://doi.org/10.1016/j.molliq.2014.07.010>.
- Selimefendigil, F., Öztop, H.F., 2016. Analysis of MHD mixed convection in a flexible walled and nanofluids filled lid-driven cavity with volumetric heat generation. *Int. J. Mech. Sci.* 118, 113–124. <https://doi.org/10.1016/j.ijmecsci.2016.09.011>.
- Abu Bakar, N., Roslan, R., Md Akhir, M.K., 2020. The effects of internal heat generation or absorption on mixed convection in a lid-driven rectangular cavity using finite volume method. *CFD Lett.* 12 (12), 38–54. <https://doi.org/10.37934/cfdl.12.12.3854>.
- Imtiaz Rais, A., Jisan Mahmud, M., Rakib Hossain, M., Saha, S., 2023. Influence of heat generation/absorption on mixed convective flow in a lid-driven chamber with isothermal rotating cylinder. *Ann. Nucl. Energy* 182. <https://doi.org/10.1016/j.anucene.2022.109596>.
- Hasan, N., Saha, S., 2024. MHD conjugate mixed convection along with internal heat generation and Joule heating in a closed/open cavity with rotating solid cylinder. *Int. J. Numer. Methods Heat Fluid Flow* 34 (9), 3438–3461. <https://doi.org/10.1108/HFF-01-2024-0054/FULL/XML>.